crystals

MDPI

Article

Thirty-Fold Increase in Relative Sensitivity of Dy^{3+} Luminescent Boltzmann Thermometers Using Multiparameter and Multilevel Cascade Temperature Readings

Željka Antić [1,*], Aleksandar Ćirić [1], Milica Sekulić [1], Jovana Periša [1], Bojana Milićević [1], Abdullah N. Alodhayb [2], Tahani A. Alrebdi [3] and Miroslav D. Dramićanin [1,*]

[1] Centre of Excellence for Photoconversion, Vinča Institute of Nuclear Sciences—National Institute of the Republic of Serbia, University of Belgrade, 11001 Belgrade, Serbia; aleksandar.ciric@ff.bg.ac.rs (A.Ć.); msekulic@vinca.rs (M.S.); jburojevic@vinca.rs (J.P.); bojana.milicevic85@gmail.com (B.M.)

[2] Department of Physics and Astronomy, College of Science, King Saud University, P.O. Box 2455, Riyadh 11451, Saudi Arabia; aalodhayb@ksu.edu.sa

[3] Department of Physics, College of Science, Princess Nourah Bint Abdulrahman University, P.O. Box 84428, Riyadh 11671, Saudi Arabia; taalrebdi@pnu.edu.sa

* Correspondence: zeljkaaa@gmail.com (Ž.A.); dramican@vinca.rs (M.D.D.)

Abstract: The sensitivity of luminescent Boltzmann thermometers is restricted by the energy difference between the thermally coupled excitement levels of trivalent lanthanides, and their values further decrease with increases in temperature, rendering their use at high temperatures difficult. Here, we demonstrate how to overcome this sensitivity limitation by employing multiparameter and multilevel cascade temperature readings. For this purpose, we synthesized Dy^{3+}:Y_2SiO_5, a phosphor whose emission is known to begin quenching at very high temperatures. Its photoluminescence-emission features, later used for thermometry, consisted of two blue emission bands centered around 486 nm and 458 nm, and two bands centered around 430 nm and 398 nm, which were only visible at elevated temperatures. Next, we performed thermometry using the standard luminescence-intensity ratio (LIR) method, which employs the $^4F_{9/2}$ and $^4I_{15/2}$ Dy^{3+} levels' emissions and the multilevel cascade method, which additionally uses the $^4G_{11/2}$ level and overlapping intensities of $^4I_{13/2}$, $^4M_{21/2}$, $^4K_{17/2}$, and $^4F_{7/2}$ levels to create two LIRs with a larger energy difference than the standard LIR. This approach yielded a sensitivity that was 3.14 times greater than the standard method. Finally, we simultaneously exploited all the LIRs in the multiparameter temperature readings and found a relative sensitivity that was 30 times greater than that of the standard approach.

Keywords: luminescence thermometry; luminescent materials; yttrium silicate; Dy^{3+}

Citation: Antić, Ž.; Ćirić, A.; Sekulić, M.; Periša, J.; Milićević, B.; Alodhayb, A.N.; Alrebdi, T.A.; Dramićanin, M.D. Thirty-Fold Increase in Relative Sensitivity of Dy^{3+} Luminescent Boltzmann Thermometers Using Multiparameter and Multilevel Cascade Temperature Readings. *Crystals* **2023**, *13*, 884. https://doi.org/10.3390/cryst13060884

Academic Editor: László Kovács

Received: 26 April 2023
Revised: 25 May 2023
Accepted: 27 May 2023
Published: 28 May 2023

1. Introduction

Temperature-induced changes in the luminescence of materials manifest in a variety of ways, such as altered emission intensity, the luminescence intensity ratio (LIR) between two emission peaks, the spectral positions of the excitation and emission bands, and excited-state lifetimes. All these alterations can be used for efficient temperature detection with a method known as luminescence thermometry [1–3]. The LIR is the most extensively used method in luminescence thermometry [4]. It plays an important role because it is self-referential and uses ratios of absolute emission intensities to avoid issues brought about by changes in measurement conditions, such as fluctuations in the excitation. When applied with lanthanide-activated phosphor probes, LIR is frequently constructed by utilizing emissions from two excited energy levels that are thermally coupled and with populations that follow the Boltzmann distribution. For this reason, the method is also known as Boltzmann thermometry. Two excited energy levels are thermally coupled when their energies are close and the nonradiative transition rates between them exceed the

radiative transition rates within the thermometer's operating range [5]. The temperature dependence of the LIR is then described by a simple exponential dependence on inverse temperature that has the form of the Boltzmann-distribution equation [6], and, accordingly, the relative sensitivity of the method, is linearly dependent on the difference in energy between emitting levels and inversely proportional to the temperature square [7,8].

The available energy levels in trivalent lanthanides limit in magnitude the relative sensitivities of the method, so they have rather good values around room temperature, such as 0.97% K^{-1} when using Pr^{3+} activated phosphor probes, 1.30% K^{-1} for Er^{3+}, 1.68% K^{-1} for Dy^{3+}, and 2.9% K^{-1} for Eu^{3+} [9]. However, the values are considerably reduced at high operating temperatures, such as only 0.18% K^{-1} for Er^{3+} and 0.22% K^{-1} for Dy^{3+} at 800 K, which makes precise temperature measurements very difficult, considering that precision is improved when uncertainty in measurement is smaller and sensitivity is larger.

The photoluminescence of Dy^{3+} is exceptionally suitable for luminescence thermometry at high temperatures. For example, Allison et al. [10] and Anderson et al. [11] showed luminescence thermometry for temperatures up to 1700 °C and 1500 °C, respectively, using $Y_3Al_5O_{12}$:Dy^{3+} luminescence. This is feasible because of the Dy^{3+} favorable energy-level structure features an energy difference of approximately ~1000 cm^{-1} between the $^4F_{9/2}$ and $^4I_{15/2}$ energy levels, and a large energy difference between the $^4F_{9/2}$ level and the highest Stark components of the $^6H_{15/2}$ ground level, of approximately 7800 cm^{-1}, which favors radiative deexcitation and efficient emission [12]. In addition, Dy^{3+} emission typically starts to quench at very high temperatures, such as at temperatures larger than 1100 °C in Y_2SiO_5 and 1250 °C in $Y_3Al_5O_{12}$ [13]. As result, luminescence thermometry using Dy^{3+} is possible using both LIR and emission-decay-temperature readouts. The former, however, has low sensitivity at high temperatures, whilst the latter necessitates more complex instrumentation and is entirely insensitive at low temperatures below that of the emission-quenching onset. To expedite their use, it is critical to improve the performance of LIR luminescence thermometers at high temperatures. The potential applications include measurements of high-temperature fields in gas flows, surface-temperature measurements of the thermal barrier and environmental barrier coatings used to protect structural materials when they operate at high temperatures, measurements of temperature of elements in operating gas turbines and internal combustion engines, heat-transfer and temperature measurements in hypersonic wind tunnels, and temperature measurements during galvanneal processes.

While uncertainty in measurements can be lowered principally by improving the instrumentation or employing instrumentation that is higher in quality, the increase in sensitivity of lanthanide luminescence thermometers is a more critical issue, and it has been the subject of recent luminescence-thermometry research. There are two main approaches to resolving this issue. The first approach is based either on the superposition of thermally coupled excited levels in the so-called multilevel cascade LIR method [14] or on the simultaneous use of thermally coupled energy-level pairs in both excitation and emission, in the recent luminescence-intensity-squared method [15,16]. So far, the sensitivity enhancement of Boltzmann thermometers using multilevel cascade LIR has been demonstrated in $Lu_{1.5}Y_{1.5}Al_5O_{12}$:$Dy^{3+}$ [17], $CaWO_4$:Dy^{3+} [18], $YAlO_3$:Dy^{3+} [19], β-$NaYF_4$:Nd^{3+} [20], YF_3:Er^{3+} [21], $YAl_3(BO_3)_4$:Pr^{3+},Gd^{3+} [22], and $Na_{0.5}La_{0.5}TiO_3$:Yb^{3+},Nd^{3+}, Y_2O_3: Yb^{3+},Nd^{3+}, and $(LiMg)_2Mo_3O_{12}$: Yb^{3+},Nd^{3+} [14]. The second approach exploits multiparameter temperature readings, advanced statistical techniques, and artificial neural networks [23–30] to account for the largest variations between photoluminescence levels collected at different temperatures to achieve the largest possible sensitivity.

Herein, we demonstrate both of the above-mentioned approaches for the enhancement of the sensitivity of a Boltzmann thermometer based on Y_2SiO_5:Dy^{3+} phosphor and compare them with the sensitivity obtained by a conventional LIR approach. Multilevel cascade thermometry was created using emissions from Dy^{3+} $^4I_{15/2}$, $^4F_{9/2}$, and overlapping emissions from $^4I_{13/2}$, $^4M_{21/2}$, $^4K_{17/2}$, and $^4F_{7/2}$ excited levels to the $^6H_{15/2}$ ground-state level, showing a relative sensitivity that was 3.14 times higher than that of the conventional LIR. Linear multiparameter temperature reading was performed using three LIRs based

on a structure with the same energy level as in the multilevel cascade approach, and a sensitivity that was 30 times larger than that of the conventional LIR was exhibited.

2. Materials and Methods

Yttrium(III) nitrate hexahydrate ($Y(NO_3)_3 \cdot 6H_2O$, Sigma Aldrich, St. Louis, MO, USA, 99.8%), dysprosium(III) nitrate pentahydrate, ($Dy(NO_3)_3 \cdot 5H_2O$, Alfa Aesar, St. Louis, MO, USA, 99.9%), SiO_2 (30mass% colloidal dispersion in ethylene glycol, 0.02-micron size), citric acid—CA ($HOC(COOH)(CH_2COOH)_2$, Sigma Aldrich, St. Louis, MO, USA, ACS reagent, ≥99.5%), and ethylene glycol—EG ($HOCH_2CH_2OH$, Sigma Aldrich, anhydrous, 99.8%) were used as preparatory materials without additional purification. The Y_2SiO_5 (YSO) sample activated with 5 mol% of Dy^{3+} ($Y_{1.9}Dy_{0.1}SiO_5$) was synthesized by a modified Pechini method (the optimal Dy^{3+} concentration was taken according to reference [31]). The desired material was obtained by dissolving stoichiometric amounts of solid metal nitrates (M) in the solution of CA in EG (M: CA: EG = 1:5:25 molar ratio); please see Table 1 for exact amounts. After mixing at 60 °C and complete dissolution of metal nitrates, a stoichiometric amount of SiO_2 colloidal dispersion in ethylene glycol was added dropwise while stirring, the temperature increased to 130 °C, and the solution was mixed for several hours until a transparent yellowish gel was formed. The level of pH was not controlled. The gel was transferred to the alumina crucible and calcined at 1000 °C for 5 h.

Table 1. Amounts of precursor materials used for the synthesis of 1 g of $Y_{1.9}Dy_{0.1}SiO_5$.

Precursor Material	Amount
$Y(NO_3)_3 \cdot 6H_2O$	2.5464 g
$Dy(NO_3)_3 \cdot 5H_2O$	0.1535 g
SiO_2 colloidal dispersion in ethylene glycol	0.54 mL
Citric acid	3.3621 g
Ethylene glycol	4.9 mL

The powder's crystal structure was investigated by X-ray diffraction (XRD) at room temperature using a Rigaku SmartLab diffractometer (Cu-K$\alpha_{1,2}$ radiation, λ = 0.1540 nm). The measurements were conducted over a range of 10° to 90°, with a step size of 0.02° and a counting time of 1°/min. The photoluminescence emission and excitation were recorded with a Horiba Jobin Yvon Fluorolog (FL3-221) spectrofluorometer through a fiber-optic bundle employing a 450-W xenon lamp as the excitation source, and the temperature of the sample was controlled by a custom-made hot-stage apparatus [32]. Emission spectra were recorded in a temperature range from 300 K to 900 K. Photoluminescence-emission decay was measured using excitation from Ocean Insight LSM-365A fiber coupled LED (10 mW maximum power), which was operated by a single-channel Ocean Insight LDC-1 driver and controller, R10467U-50 hybrid photo detector comprising the H10722-20 photosensor module with PMT, and RTC1002EDU oscilloscope (Rohde and Schwarz). Built-in MATLAB 2021b functions (University of Belgrade licence) were used to perform all calculations.

3. Results

3.1. Crystal Structure of $Y_{1.9}Dy_{0.1}SiO_5$ Luminescence Probe

Figure 1 shows the diffraction pattern for the $Y_{1.9}Dy_{0.1}SiO_5$ powder sample, which corresponded to a monoclinic crystal structure with the P21/c space group. All the diffraction peaks matched well with the ICDD card no. 01-070-5613, with no peaks indicating impurities or the formation of other phases. Since the ionic radii of the Y^{3+} and Dy^{3+} were very similar (1.027 Å and 1.019 Å, respectively), the X-ray pattern indicated that the Dy^{3+} was successfully incorporated into the Y_2SiO_5 crystal lattice. Using the built-in PDXL2 software, the average crystallite size and structural parameters (Table 2) were determined; the initial parameters for the analysis were obtained from [33].

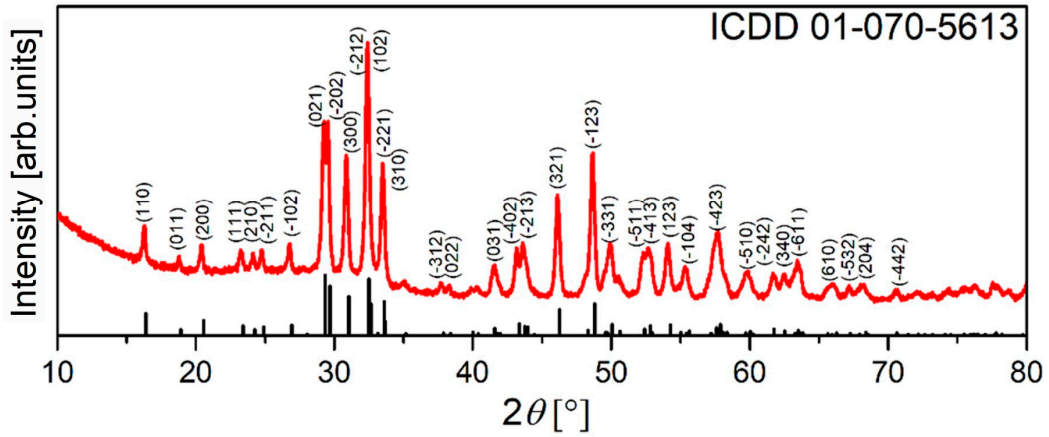

Figure 1. X-ray diffraction pattern of $Y_{1.9}Dy_{0.1}SiO_5$ phosphor powder. The diffraction peaks are indexed with respect to ICDD card no. 01-070-5613.

Table 2. The structural parameters of the $Y_{1.9}Dy_{0.1}SiO_5$ phosphor powder.

ICDD Card 01-070-5613	$Y_{1.9}Dy_{0.1}SiO_5$
Crystallite size (nm)	20.7(3)
Strain	0.16(8)
Rwp *	7.26
Re *	3.18
GOF *	2.2806
a (Å)	9.0364(11)
b (Å)	6.9353(8)
c (Å)	6.6602(8)

* Rwp—the weighted profile factor; Re—the expected weighted profile factor; GOF—the goodness of fit.

3.2. Temperature Dependence of Y_2SiO_5:Dy^{3+} Photoluminescence

Figure 2a depicts the excitation spectrum of $Y_{1.9}Dy_{0.1}SiO_5$ obtained by measuring the intensity of the 486-nm emission peak corresponding to the Dy^{3+} $^4F_{9/2} \rightarrow ^6H_{15/2}$ transition. Two intense absorption bands were observed at 353 nm and 364 nm in the near-ultraviolet region of the spectrum [34,35]. These absorptions were typical for Dy^{3+}-activated phosphors. When electrons were excited with 353 nm, they de-excited to the $^4I_{15/2}$ level. The competing radiative and nonradiative processes facilitated the thermalization of excited levels. The exponential decay with time of the $^4F_{9/2}$ emission measured at room temperature (λex = 353 nm, λem = 484 nm) is shown in Figure 2b. The lifetime value calculated from the decay was 350 ± 17 μs (average of 30 measurements) and agreed with the data in the literature for the Y_2SiO_5 activated by a similar amount of Dy [36]. The energy-level diagram with observed emissions and the corresponding energy differences between the energy levels that provided these emissions are shown in Figure 2c.

Figure 2d–f show the emission spectra recorded at different temperatures over the 300–900 K range (λ_{ex}= 353 nm). The emissions due to the $^4G_{11/2} \rightarrow ^6H_{15/2}$ transition started to appear at around 430 nm at temperatures higher than 550 K, while the overlapping emissions from the higher-energy-thermalized levels ($^4I_{13/2}$, $^4M_{21/2}$, $^4K_{17/2}$, and $^4F_{7/2} \rightarrow ^6H_{15/2}$) became visible at around 398 nm at temperatures above 650 K (Figure 2d,e). As shown by the presented spectra, $^4I_{15/2} \rightarrow ^6H_{15/2}$, $^4G_{11/2} \rightarrow ^6H_{15/2}$ and the $^4I_{13/2}$, $^4M_{21/2}$, $^4K_{17/2}$, and $^4F_{7/2} \rightarrow ^6H_{15/2}$ emission intensities increased in line with the temperature increase. Characteristic emission peaks from Dy^{3+} $^4I_{15/2} \rightarrow ^6H_{15/2}$ and $^4F_{9/2} \rightarrow ^6H_{15/2}$ transitions can be seen at the wavelengths centered at 458 nm and 483 nm, respectively (Figure 2f).

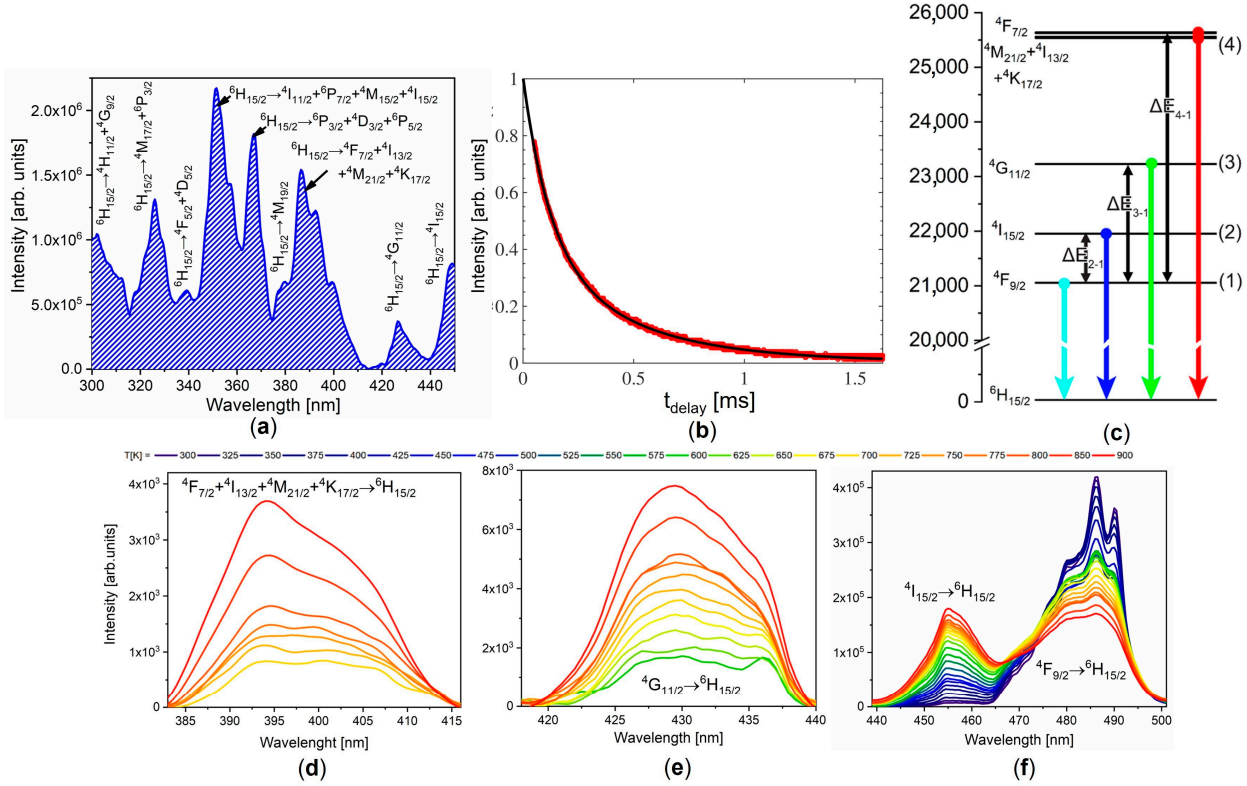

Figure 2. (**a**) Excitation spectrum of $Y_{1.9}Dy_{0.1}SiO_5$ recorded by monitoring the intensity of 486 nm emissions; (**b**) exponential decay of the $^4F_{9/2}$ emissions measured at room temperature (λex = 353 nm, λem = 484 nm); (**c**) diagram of Dy^{3+} energy levels with marked transitions used for different luminescence intensity ratios (LIR_{2-1}, LIR_{3-1}, and LIR_{4-1}) and the corresponding energy differences ΔE_{2-1}, ΔE_{3-1}, and ΔE_{4-1}; (**d**) temperature dependence of the $^4I_{13/2}$, $^4M_{21/2}$, $^4K_{17/2}$, and $^4F_{7/2}\rightarrow{}^6H_{15/2}$ emissions; (**e**) temperature dependence of the $^4G_{11/2}\rightarrow{}^6H_{15/2}$ emissions spectrum; (**f**) temperature dependence of $^4F_{7/2}\rightarrow{}^6H_{15/2}$ and $^4I_{15/2}\rightarrow{}^6H_{15/2}$ emissions spectra. All emission spectra were measured under λex = 353 nm excitation.

3.3. Conventional and Multilevel Cascade LIR Temperature Readings

The ratio of the emission intensities (*LIR*) from the excited levels that are in thermal equilibrium is described by [6]:

$$LIR = \frac{I_H}{I_L} = Be^{-\frac{\Delta E}{kT}}, \quad (1)$$

where I_H and I_L represent the emission intensities from higher and lower energy levels. The ΔE is the difference in energy between these levels, and $k = 0.695\ cm^{-1}K^{-1}$ is the Boltzmann constant. The pre-exponential factor B accounts for the degeneracy of the excited levels g, the spontaneous emission rates A, and the energy of the transition $h\nu$:

$$B = \frac{g_H A_H h\nu_H}{g_L A_L h\nu_L}. \quad (2)$$

Equation (1) takes into account only the ratio of the Boltzmann equilibrium levels' populations. Considering that the temperature quenching of luminescence intensity is negligible at the investigated temperature range for Y_2SiO_5:Dy^{3+}, one can safely neglect the luminescence intensity's dependance on the probability of the mutiphonon non-radiative relaxation of the excited states (each excited state has its own probability).

The relative sensitivity (S_R) is a figure of merit in thermometry that signifies the degree to which a temperature indicator varies with temperature. It critically influences

the uncertainty in the temperature determination and is commonly used to compare the performances of luminescence-thermometry methods and probes. When considering the mathematical representation of the *LIR* given by Equation (1), the relative sensitivity of the *LIR* method is:

$$S_R\left[\%\ \mathrm{K}^{-1}\right] = \frac{1}{LIR}\left|\frac{\partial LIR}{\partial T}\right| \cdot 100\% = \frac{\Delta E}{kT^2} \cdot 100\%. \quad (3)$$

According to this expression, larger values of relative sensitivity are obtained when using the ratio of the emissions from thermalized levels with larger differences in energy. In addition, the relative sensitivity values decrease rapidly with increases in temperature.

The conventional LIR approach uses the emissions from two neighboring excited levels. For Dy^{3+}, it is constructed from the $^4I_{15/2} \rightarrow {}^6H_{15/2}/{}^4F_{9/2} \rightarrow {}^6H_{15/2}$ emissions-intensity ratio. We denote it here as $LIR_{2\text{-}1}$, with the corresponding difference in energy among the levels of $\Delta E_{2\text{-}1}$ (see Figure 2b). It was measured over the entire temperature range (300–900 K), and it is represented graphically in Figure 3a. The fit of Equation (1) with the experimental data is depicted with a solid line in Figure 3a, while the data obtained from the fit are provided in Table 3. According to Equation (3), the relative sensitivity of the method was 1.85% K^{-1} at 300 K (around room temperature) but decreased almost ninefold to 0.21% K^{-1} at 900 K (Figure 3d).

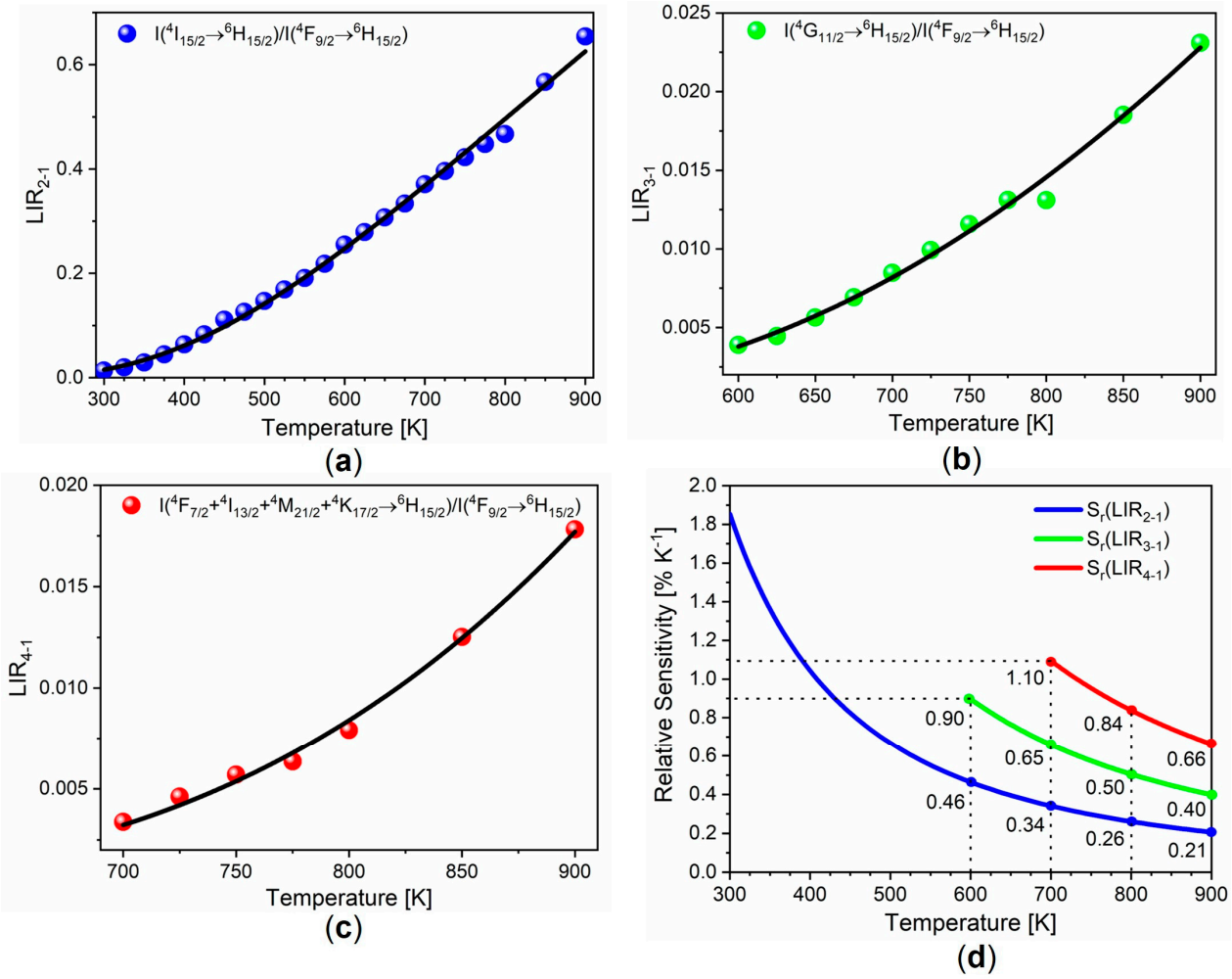

Figure 3. Temperature dependence of three different luminescence-intensity ratios: (**a**) $LIR_{2\text{-}1}$, (**b**) $LIR_{3\text{-}1}$, and (**c**) $LIR_{4\text{-}1}$; (**d**) relative sensitivity values obtained by $LIR_{2\text{-}1}$, $LIR_{3\text{-}1}$, and $LIR_{4\text{-}1}$ temperature readouts. Note that error bars are smaller than the sizes of symbols. The LIR temperature dependences were fitted by LumTHools software [37].

Table 3. Parameters obtained from fitting experimental LIR data to Equation (1) for the conventional LIR ($LIR_{3\text{-}1}$) and multilevel cascade LIRs ($LIR_{3\text{-}1}$ and $LIR_{4\text{-}1}$), along with temperature ranges of measurements and values of relative sensitivities at 900 K.

	B	ΔE (cm^{-1})	Adj. R^2	Temperature Range (K)	Relative Sensitivity at 900 K (% K^{-1})
$LIR_{2\text{-}1}$	3.99 ± 0.17	1160 ± 21	0.997	300–900	0.21
$LIR_{3\text{-}1}$	0.82 ± 0.11	2244 ± 77	0.992	600–900	0.40
$LIR_{4\text{-}1}$	6.90 ± 1.50	3728 ± 131	0.994	700–900	0.66

The multilevel cascade LIR based on the integrated emissions from the $^4I_{15/2}$ and $^4G_{11/2}$ levels, $LIR_{3\text{-}1}$, was measured in the 600–900-K temperature range, and it is depicted in Figure 3b with symbols. The fit with Equation (1) is represented by the solid line in Figure 3b, and the data obtained from the fit are listed in Table 3. The large energy difference between the excited levels ($\Delta E_{3\text{-}1}$ in Figure 2b) at 2244 cm^{-1} necessitates high temperatures to populate the $^4G_{11/2}$ level, whose emission was visible at 550 K and reliably measurable at temperatures above 600 K. The greater energy difference between the excited levels in the $LIR_{3\text{-}1}$ compared to the conventional LIR resulted in greater relative sensitivity values. At 900 K, the value was 0.40% K^{-1}, which was twice as high as in the LIR (Figure 3d).

The overlapping emissions from the closely spaced $^4I_{13/2}$, $^4M_{21/2}$, $^4K_{17/2}$, and $^4F_{7/2}$ excited levels (see Figure 2b) and the emissions from the $^4F_{9/2} \rightarrow {}^6H_{15/2}$ transition provided the multilevel cascade LIR ($LIR_{4\text{-}1}$) with an even greater energy difference ($\Delta E_{4\text{-}1}$) of 3728 cm^{-1}. The results of the fitting of the experimental data to Equation (1) over the 700–900-K temperature range are depicted graphically in Figure 3c, and the data are provided in Table 3. The relative sensitivity of 0.66% K^{-1} at 900 K was 3.14 times larger than in the traditional LIR (see Figure 3d).

3.4. Multiparameter Temperature Readout

Multiple luminescence phenomena that vary with temperature are utilized simultaneously in multiparameter thermometry. Maturi et al. [24] recently incorporated multiparametric linear regression (*MLR*) into luminescence thermometry to improve the performance of luminescence thermometers by a factor of ten using, for example, the intensity ratio of two emissions bands, band energies, and bandwidths. In *MLR* luminescence thermometry, the reference temperature is equal to the sum of the distinct functions of the indications in the measurement, Δ_i (parameters such as LIR functions, lifetime functions, bandshift functions, etc.), and their weighting factors, β_i:

$$T = \beta_0 + \sum_{i=1}^{n} \beta_i \Delta_i + \varepsilon, \tag{4}$$

where $\sum_i \beta_i = 1$, β_0 is the intercept in the n-dimensional space of the fitting parameters, and ε represents the residuals. According to Maturi et al. [24], the relative sensitivity of the method is:

$$S_r^{MLR} = \sqrt{\sum_{i=1}^{n} S_{r_i}^2} = \sqrt{\sum_{i=1}^{n} \frac{1}{\beta_i^2 \Delta_i^2}}. \tag{5}$$

We constructed the multiparameter luminescence thermometry by applying *MLR* to three LIRs ($LIR_{2\text{-}1}$, $LIR_{3\text{-}1}$, and $LIR_{4\text{-}1}$) over the temperature range of 700–900 K, assuming that all the required emissions were measurable in this temperature range. To produce a linear relationship between the indicators and the temperature, which is a prerequisite for using *MLR*, and feature scaling, which allows the fitting of indicators with similar magnitudes, we derived the following indicator functions from Equation (1):

$$\Delta_i = \frac{\Delta E_i}{k \cdot [\log(B_i) - \log(LIR_i)]}, \quad i \in \{2\text{-}1,\ 3\text{-}1,\ 4\text{-}1\}. \tag{6}$$

Table 4 displays the outcome of the *MLR* fitting of the experimental data to Equation (4) (the residual ε was negligible). Considering that each Δ_i represents the temperature (see Equations (1) and (6)), the relative sensitivity equation, Equation (6) [24], can be formulated as follows:

$$S_r^{MLR} = \sqrt{S_{r_{2-1}}^2 + S_{r_{3-1}}^2 + S_{r_{4-1}}^2} = \frac{1}{T}\sqrt{\frac{1}{\beta_{2-1}^2} + \frac{1}{\beta_{3-1}^2} + \frac{1}{\beta_{4-1}^2}}. \quad (7)$$

Therefore, the relative sensitivity of this multiparameter temperature readout depends on the inverse temperature and β coefficients, and the Y_2SiO_5:Dy^{3+} system of three LIRs is equal to

$$S_r^{MLR}\left[\%\,K^{-1}\right] = \frac{63.65}{T}\cdot 100\%. \quad (8)$$

Figure 4 depicts the relative sensitivity values of the *MLR* method (black line), the multilevel cascade method (MLC, red line), and the conventional LIR (blue line). The relative sensitivity of the *MLR* method was 9.05% K^{-1} at 700 K and 7.04% K^{-1} at 900 K. The *MLR* method had a relative sensitivity of 9.05% K^{-1} at 700 K and 7.04% K^{-1} at 900 K. It was, on average, 30 times greater than the relative sensitivity of the conventional LIR throughout the entire temperature range (26.6 times greater at 700 K and 33.5 times greater at 900 K).

Table 4. Parameters used in MLR and the weighting coefficients for MLR using three LIRs.

i	*B*	Δ*E*	β_i
2-1	3.99	1160	0.0179
3-1	0.82	2244	0.0328
4-1	6.90	3728	0.9489

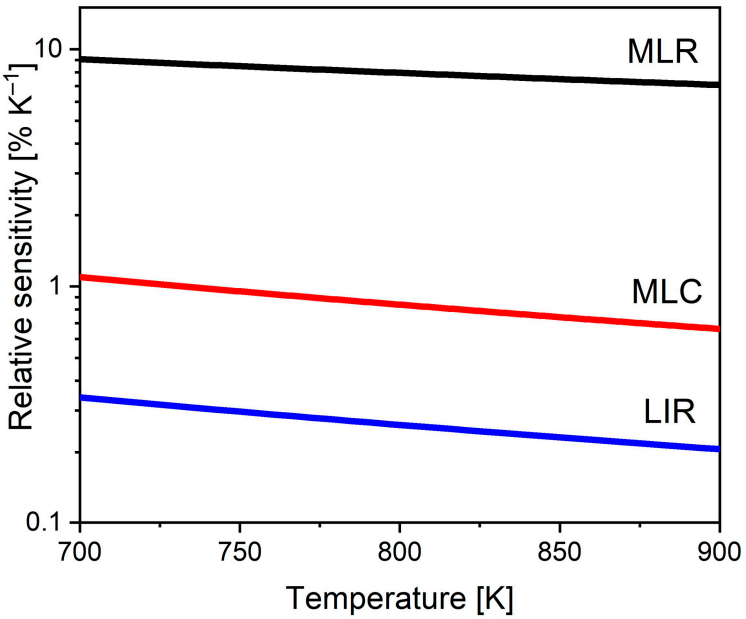

Figure 4. Comparison of relative sensitivities of multiparameter (MLR, black line), multilevel cascade (MLC, red line), and conventional LIR (blue line) thermometry. Note that sensitivity of MLR is proportional to T^{-1}, while MLC and LIR are proportional to T^{-2}.

4. Discussion

Using a multilevel cascade LIR approach, the relative sensitivity of luminescence thermometry with the Y_2SiO_5:Dy^{3+} phosphor can be enhanced, similar to recent reports discussing thermometry with other lanthanide phosphors [14,17–22]. Due to the large

energy difference (3728 cm^{-1}) between the Dy^{3+} $^4F_{9/2}$ level and the group of closely spaced excited levels ($^4I_{13/2}$, $^4M_{21/2}$, $^4K_{17/2}$, and $^4F_{7/2}$), the relative sensitivity enhancement in this instance was substantial, 3.14 times the value of the conventional LIR sensitivity. However, the method could not be used at temperatures below 700 K, as the emission intensities from the high-energy-excited levels were too weak to be reliably measured at these temperatures. On the other hand, the intensity of these emissions increased continuously as the temperature increased, and they were measured at temperatures greater than 900 K, up to the point at which the emission quenching began. This suggests that the method's application at very high temperatures is extremely promising. For this purpose, phosphors that are chemically and thermally stable with high temperature-emission-quenching onset should be used, such as rare-earth garnets, phosphates, vandates, silicates, and yttrium-stabilized zirconia [13,38,39]. Unfortunately, due to the limitations of our instruments, we were unable to conduct measurements at temperatures exceeding 900 K.

Using a combination of multiparametric linear regression and multilevel cascade LIR, the relative sensitivity of thermometry at high temperatures can be increased by at least 30 times compared to conventional LIR thermometry with Dy^{3+}. In addition, in this method, the relative sensitivity decreases with increases in temperature proportional to T^{-1} rather than T^{-2}, as in conventional LIR. As a result, the difference between the sensitivity values becomes larger as temperatures increase further. For instance, based on Equations (3) and (8), the sensitivity of this procedure at 1200 K is 5.3% K^{-1}, while the sensitivity of the LIR is 0.16% K^{-1}. At 1500 K, this method's sensitivity is 4.24% K^{-1}, which is 57.3 times greater than the conventional LIR sensitivity of 0.07% K^{-1}.

In this investigation, we were only concerned with the improvement in the relative sensitivity brought about by the proposed methods. Uncertainty in measurement and repeatability are predominantly dependent on the characteristics of the instruments used and, to a much lesser extent, on the procedure used to determine the temperature from the luminescence. A further comprehensive study involving instruments with different performances is planned to assess the range of values of measurement uncertainty and repeatability. Nevertheless, based on the fact that the intensities of the emissions from the high-energy-excited states continued to increase as the temperature rose, it is reasonable to anticipate that uncertainties in the measurement of emission intensities are comparable with or even lower than those in the conventional LIR.

5. Conclusions

The sensitivity of multilevel cascade LIR thermometry is greatly superior to that of traditional luminescence-intensity-ratio thermometry when used either alone or in conjunction with multiparametric linear regression. The latter increases the sensitivity by a factor of 30 between, 700 K and 900 K. The essential characteristic of this approach is that the relative sensitivity decreases with increases in temperature much more slowly than in conventional LIR, since it is proportional to T^{-1} rather than T^{-2}, as in conventional LIR. This method requires the use of chemically and thermally stable phosphor with emission-quenching onset at very high temperatures. These conditions were fulfilled with the Y_2SiO_5:Dy^{3+} phosphor used in this study. The emission of Dy^{3+} is particularly well suited to both conventional and multilevel cascade LIR thermometry due to its ladder-like structure of excited levels, with energy differences that may be easily thermalized. Furthermore, the Dy^{3+} emissions used for temperature determination are in the near-ultraviolet and blue spectral regions, where the impact of Planck radiation is much smaller than at longer wavelengths, where other trivalent lanthanide ions are emitted. The main disadvantage of this approach is that it cannot be employed at low temperatures due to a lack of energy for the thermalization of high-energy-excited states. However, at low temperatures, the standard LIR based on Dy^{3+} emissions is sufficiently sensitive. In the future, we intend to thoroughly analyze the uncertainties in this method's temperature determination using instrumentation with different characteristics. Furthermore, we intend to apply several

modern statistical and machine-learning methods, such as principal component analysis and artificial neural networks, to test the improvements in the performance of traditional and multilevel cascade LIR thermometry.

Author Contributions: Conceptualization, M.D.D.; methodology, Ž.A., A.Ć. and M.D.D.; validation, A.N.A., T.A.A. and Ž.A.; formal analysis, T.A.A., A.N.A. and A.Ć.; investigation, A.Ć., J.P., M.S., B.M. and T.A.A.; resources, M.D.D.; data curation, A.Ć.; writing—original draft preparation, M.D.D.; writing—review and editing, M.D.D.; visualization, A.Ć. and Ž.A.; funding acquisition, A.N.A. and M.D.D. All authors have read and agreed to the published version of the manuscript.

Funding: This research was funded by the NATO Science for Peace and Security Program under grant ID G5751. This research was also funded by Princess Nourah bint Abdulrahman University, Riyadh, Saudi Arabia, Princess Nourah bint Abdulrahman University Researchers Supporting Project Number PNURSP2023R71. Author Abdullah Alodhayb acknowledges Researchers Supporting Project Number RSP2023R304, King Saud University, Riyadh, Saudi Arabia. This research was also funded by Ministry of Science, Technological Development and Innovation of the Republic of Serbia under contract 451-03-47/2023-01/200017.

Data Availability Statement: Data and spectra presented in this study are available from Zenodo DOI: 10.5281/zenodo.7866010.

Conflicts of Interest: The authors declare no conflict of interest. The funders had no role in the design of the study; in the collection, analyses, or interpretation of data; in the writing of the manuscript; or in the decision to publish the results.

References

1. Allison, S.W. A brief history of phosphor thermometry. *Meas. Sci. Technol.* **2019**, *30*, 072001. [CrossRef]
2. Dramićanin, M. Schemes for Temperature Read-Out from Luminescence. In *Luminescence Thermometry*; Elsevier: Amsterdam, The Netherlands, 2018; pp. 63–83.
3. Quintanilla, M.; Benayas, A.; Naccache, R.; Vetrone, F. Luminescent Nanothermometry with Lanthanide-doped Nanoparticles. In *Thermometry at the Nanoscale*; Royal Society of Chemistry: London, UK, 2015; pp. 124–166.
4. Brites, C.D.S.; Balabhadra, S.; Carlos, L.D. Lanthanide-Based Thermometers: At the Cutting-Edge of Luminescence Thermometry. *Adv. Opt. Mater.* **2018**, *7*, 1801239. [CrossRef]
5. Geitenbeek, R.G.; de Wijn, H.W.; Meijerink, A. Non-Boltzmann Luminescence in $NaYF_4$:Eu^{3+}: Implications for Luminescence Thermometry. *Phys. Rev. Appl.* **2018**, *10*, 64006. [CrossRef]
6. Wade, S.A.; Collins, S.F.; Baxter, G.W. Fluorescence intensity ratio technique for optical fiber point temperature sensing. *J. Appl. Phys.* **2003**, *94*, 4743–4756. [CrossRef]
7. Dramićanin, M.D. Trends in luminescence thermometry. *J. Appl. Phys.* **2020**, *128*, 40902. [CrossRef]
8. Dramićanin, M.D. Sensing temperature via downshifting emissions of lanthanide-doped metal oxides and salts. A review. *Methods Appl. Fluoresc.* **2016**, *4*, 042001. [CrossRef]
9. Dramićanin, M. Lanthanide and Transition Metal Ion Doped Materials for Luminescence Temperature Sensing. In *Luminescence Thermometry*; Elsevier: Amsterdam, The Netherlands, 2018; p. 137.
10. Allison, S.W.; Beshears, D.L.; Cates, M.R.; Scudiere, M.B.; Shaw, D.W.; Ellis, A.D. Luminescence of YAG:Dy and YAG:Dy,Er crystals to 1700 °C. *Meas. Sci. Technol.* **2019**, *31*, 044001. [CrossRef]
11. Anderson, B.R.; Livers, S.; Gunawidjaja, R.; Eilers, H. Fiber-based optical thermocouples for fast temperature sensing in extreme environments. *Opt. Eng.* **2019**, *58*, 097105. [CrossRef]
12. Aldén, M.; Omrane, A.; Richter, M.; Särner, G. Thermographic phosphors for thermometry: A survey of combustion applications. *Prog. Energy Comb. Sci.* **2011**, *37*, 422–461. [CrossRef]
13. Chambers, M.D.; Clarke, D.R. Doped Oxides for High-Temperature Luminescence and Lifetime Thermometry. *Annu. Rev. Mater. Res.* **2009**, *39*, 325–359. [CrossRef]
14. Wang, Y.; Sun, Y.; Xia, Z. Energy Gap Linear Superposition of Thermally Coupled Levels toward Enhanced Relative Sensitivity of Ratiometric Thermometry. *J. Phys. Chem. Lett.* **2023**, *14*, 178–182. [CrossRef]
15. Ćirić, A.; Marciniak, Ł.; Dramićanin, M.D. Luminescence intensity ratio squared—A new luminescence thermometry meth-od for enhanced sensitivity. *J. Appl. Phys.* **2022**, *131*, 114501. [CrossRef]
16. Ćirić, A.; van Swieten, T.; Periša, J.; Meijerink, A.; Dramićanin, M.D. Twofold increase in the sensitivity of Er3+/Yb3+ Boltzmann thermometer. *J. Appl. Phys.* **2023**, *133*, 194501. [CrossRef]
17. Ćirić, A.; Periša, J.; Zeković, I.; Antić, Ž.; Dramićanin, M.D. Multilevel-cascade intensity ratio temperature read-out of Dy^{3+} luminescence thermometers. *J. Lumin.* **2022**, *245*, 118795. [CrossRef]
18. Li, L.; Qin, F.; Zhou, Y.; Zheng, Y.; Miao, J.; Zhang, Z. Three-energy-level-cascaded strategy for a more sensitive luminescence ratiometric thermometry. *Sens. Actuator A Phys.* **2020**, *304*, 111864. [CrossRef]

19. Periša, J.; Ćirić, A.; Zeković, I.; Đorđević, V.; Sekulić, M.; Antić, Ž.; Dramićanin, M.D. Exploiting High-Energy Emissions of $YAlO_3$:Dy^{3+} for Sensitivity Improvement of Ratiometric Luminescence Thermometry. *Sensors* **2022**, *22*, 7997. [CrossRef] [PubMed]
20. Tian, X.; Wei, X.; Chen, Y.; Duan, C.; Yin, M. Temperature sensor based on ladder-level assisted thermal coupling and thermal-enhanced luminescence in $NaYF_4$: Nd^{3+}. *Opt. Express* **2014**, *22*, 30333–30345. [CrossRef] [PubMed]
21. Ćirić, A.; Aleksić, J.; Barudžija, T.; Antić, Ž.; Đorđević, V.; Medić, M.; Periša, J.; Zeković, I.; Mitrić, M.; Dramićanin, M.D. Comparison of three ratiometric temperature readings from the Er^{3+} upconversion emission. *Nanomaterials* **2020**, *10*, 627. [CrossRef] [PubMed]
22. Yu, D.; Li, H.; Zhang, D.; Zhang, Q.; Meijerink, A.; Suta, M. One ion to catch them all: Targeted high-precision Boltzmann thermometry over a wide temperature range with Gd^{3+}. *Light Sci. Appl.* **2021**, *10*, 236. [CrossRef]
23. Shen, Y.; Santos, H.D.A.; Ximendes, E.C.; Lifante, J.; Sanz-Portilla, A.; Monge, L.; Fernández, N.; Chaves-Coira, I.; Jacinto, C.; Brites, C.D.S.; et al. Ag_2S Nanoheaters with Multiparameter Sensing for Reliable Thermal Feedback during In Vivo Tumor Therapy. *Adv. Funct. Mater.* **2020**, *30*, 2002730. [CrossRef]
24. Maturi, F.E.; Brites, C.D.S.; Ximendes, E.C.; Mills, C.; Olsen, B.; Jaque, D.; Ribeiro, S.J.L.; Carlos, L.D. Going Above and Beyond: A Tenfold Gain in the Performance of Luminescence Thermometers Joining Multiparametric Sensing and Multiple Regression. *Laser Photonics Rev.* **2021**, *15*, 2100301. [CrossRef]
25. Aseev, V.A.; Borisevich, D.A.; Khodasevich, M.A.; Kuz'menko, N.K.; Fedorov, Y.K. Calibration of Temperature by Normalized Up-Conversion Fluorescence Spectra of Germanate Glasses and Glass Ceramics Doped with Erbium and Ytterbium Ions. *Opt. Spectrosc.* **2021**, *129*, 297–302. [CrossRef]
26. Borisov, E.V.; Kalinichev, A.A.; Kolesnikov, I.E. ZnTe Crystal Multimode Cryogenic Thermometry Using Raman and Luminescence Spectroscopy. *Materials* **2023**, *16*, 1311. [CrossRef] [PubMed]
27. Ximendes, E.; Marin, R.; Carlos, L.D.; Jaque, D. Less is more: Dimensionality reduction as a general strategy for more precise luminescence thermometry. *Light Sci. Appl.* **2022**, *11*, 237. [CrossRef]
28. Liu, L.; Zhong, K.; Munro, T.; Alvarado, S.; Côte, R.; Creten, S.; Fron, E.; Ban, H.; Van der Auweraer, M.; Roozen, N.B.; et al. Wideband fluorescence-based thermometry by neural network recognition: Photothermal application with 10 ns time resolution. *J. Appl. Phys.* **2015**, *118*, 184906. [CrossRef]
29. Lewis, C.; Erikson, J.W.; Sanchez, D.A.; McClure, C.E.; Nordin, G.P.; Munro, T.R.; Colton, J.S. Use of Machine Learning with Temporal Photoluminescence Signals from CdTe Quantum Dots for Temperature Measurement in Microfluidic Devices. *ACS Appl. Nano Mater.* **2020**, *3*, 4045–4053. [CrossRef] [PubMed]
30. Cui, J.; Xu, W.; Yao, M.; Zheng, L.; Hu, C.; Zhang, Z.; Sun, Z. Convolutional neural networks open up horizons for luminescence thermometry. *J. Lumin.* **2023**, *256*, 119637. [CrossRef]
31. Dhanalakshmi, K.; Hari Krishna, R.; Jagannatha Reddy, A.; Chandraprabha, M.N.; Monika, D.L.; Parashuram, L. Photo- and thermoluminescence properties of single-phase white light-emitting $Y_{2-x}SiO_5$:xDy^{3+} nanophosphor: A concentration-dependent structural and optical study. *Appl. Phys. A* **2019**, *125*, 526. [CrossRef]
32. Ćirić, A.; Stojadinović, S.; Dramićanin, M.D. Custom-built thermometry apparatus and luminescence intensity ratio thermometry of ZrO_2:Eu^{3+} and Nb_2O_5:Eu^{3+}. *Meas. Sci. Technol.* **2019**, *30*, 045001. [CrossRef]
33. Wang, J.; Tian, S.; Li, G.; Liao, F.; Jing, X. Preparation and X-ray characterization of low-temperature phases of R_2SiO_5 (R = rare earth elements). *Mater. Res. Bull.* **2001**, *36*, 1855–1861. [CrossRef]
34. Carnall, W.T.; Fields, P.R.; Rajnak, K. Electronic Energy Levels in the Trivalent Lanthanide Aquo Ions. I. Pr^{3+}, Nd^{3+}, Pm^{3+}, Sm^{3+}, Dy^{3+}, Ho^{3+}, Er^{3+}, and Tm^{3+}. *J. Chem. Phys.* **1968**, *49*, 4424–4442. [CrossRef]
35. Ishiwada, N.; Fujii, E.; Yokomori, T. Evaluation of Dy-doped phosphors (YAG:Dy, Al_2O_3:Dy, and Y_2SiO_5:Dy) as thermographic phosphors. *J. Lumin.* **2018**, *196*, 492–497. [CrossRef]
36. Chepyga, L.M.; Hertle, E.; Ali, A.; Zigan, L.; Osvet, A.; Brabec, C.J.; Batentschuk, M. Synthesis and Photoluminescent Properties of the Dy^{3+} Doped YSO as a High-Temperature Thermographic Phosphor. *J. Lumin.* **2018**, *197*, 23–30. [CrossRef]
37. Ćirić, A.; Dramićanin, M.D. LumTHools—Software for fitting the temperature dependence of luminescence emission intensity, lifetime, bandshift, and bandwidth and luminescence thermometry and review of the theoretical models. *J. Lumin.* **2022**, *252*, 119413. [CrossRef]
38. Chepyga, L.M.; Osvet, A.; Brabec, C.J.; Batentschuk, M. High-temperature thermographic phosphor mixture YAP/YAG:Dy^{3+} and its photoluminescence properties. *J. Lumin.* **2017**, *188*, 582–588. [CrossRef]
39. Skinner, S.J.; Feist, J.P.; Brooks, I.J.E.; Seefeldt, S.; Heyes, A.L. YAG:YSZ composites as potential thermographic phosphors for high temperature sensor applications. *Sens. Actuators B Chem.* **2009**, *136*, 52–59. [CrossRef]